minerals

MDPI

Article

Volcanic and Saline Lithium Inputs to the Salar de Atacama

Linda Godfrey [1,*] and Fernanda Álvarez-Amado [2,3]

[1] Department of Earth and Planetary Sciences, Rutgers University, Piscataway, NJ 08504, USA
[2] Departamento de Ciencias de la Tierra, Universidad de Concepcion, Casilla 160-C, Concepcion 78349, Chile; fernandaalvarez@udec.cl
[3] Millennium Nucleus for Metal Tracing along Subduction, FCFM, Universidad de Chile, Santiago 758-0150, Chile
* Correspondence: lvgodfre@eps.rutgers.edu

Received: 1 January 2020; Accepted: 17 February 2020; Published: 24 February 2020

Abstract: The Li-rich brine contained within the halite body of the Salar de Atacama is uncommon for two reasons: First, it has an exceptionally high Li concentration, even compared to other closed basins in the Li triangle of South America; and second, it is widespread within the halite nucleus and not restricted to a localized area. This study focusses on the southern half of the salar where Li production occurs and draws comparisons with its northern neighboring basin through which the Loa river flows. Concentration and isotope data for water inflowing to this part of the salar were obtained from surface inflow as well as wells located within the alluvial fans on its eastern margin. Lithium varies between 0.2 and 20 mg/L before reaching the salar where small amounts of the brine and or salts that precipitated from it can increase its concentration up to 400 mg/L or higher. The δ^7Li of the inflow water varies between +4.9‰ and +11.2‰ and increases to +12.6‰ within the salar margin, consistent with salar brine based on reported measurements. Boron isotopes indicate that it is unlikely that solutes are derived from sedimentary evaporites or mineral cements, unlike the situation in the adjacent Loa basin. Water that flows through an aquifer laterally confined by a basement block and a line of volcanoes has a notably higher δ^7Li than other inflow water, around +9‰, and increasing to +10.5‰. δ^7Li values are overall higher than were measured in the adjacent Loa basin, indicating that here the water–rock reactions for Li are more evolved due to longer residence times. Lithium concentrations increased with sodium and chloride, but sedimentary evaporites are shown to be unimportant from δ^{11}B. This is accounted for two ways: evaporated saline inflow leaks from higher elevation basins and inflows are partly derived from or modified by active volcanic systems. Active and dormant volcanoes plus the massive Altiplano–Puna magmatic body are important as heat sources, which enhance water–rock reactions. The large topographic difference between the mean elevation of Altiplano on which these volcanoes sit and the salar surface allows hydrothermal fluids, which would otherwise stay deep below the surface under the modern arc, to uplift at the salar.

Keywords: lithium isotopes; boron isotopes; volcanism; water–rock interaction

1. Introduction

The Salar de Atacama is extraordinary because Li has become extremely enriched in the interstitial brine of its halite nucleus. Li concentrations exceed 1000 mg/L nearly everywhere, and in its southern sector, close to the Cordón de Lila, they reach 5000 mg/L [1]. Its average concentration of 1400 mg/L exceeds the Li concentrations of other salars in the region by a factor of four, with the possible exception of Pastos Grandes in Bolivia, which averages 1062 mg/L [2,3] though its spatial extent is not reported. Hypotheses why Li becomes so enriched in brine within closed basins of the central

Andes include indeterminate Li-rich rocks or clays, hydrothermal activity, an arid climate and tectonic subsidence [2–8]. These hypotheses are characteristic of the area in general, and not specific to the Salar de Atacama; thus, the reasons why the Salar de Atacama has become exceptionally enriched in Li requires a specific set of conditions.

The Salar de Atacama has been studied extensively. Data for surface water inflow to the halite nucleus are readily available [9–12], but for deeper inflow and the salar brine data, the data are proprietary or without spatial identification [1]. Isotopic information can provide insight into the chemical processes beyond that based on chemical concentrations, but isotope data are sparse. Li isotope data have only been reported for water at the end of a single aquifer, which drains into the salar in its southeastern corner [1], and so cannot be representative of the whole system. This study also focusses on a part of the salar, its broader southern half and drainage system, because this part of the salar is where most of the extraction of the Li brine occurs. In addition to the Li isotopes, we include the B and Sr isotope systems studied in the neighboring upper Loa basin [13]. Li and B isotopic tracers are strongly influenced by geochemical processes, such as temperatures of weathering and formation of secondary phases. Evaporation involves minimal isotope fractionation of dissolved Li, partly because so little is removed into evaporite minerals, including halite [5]. Boron, like Li, is considered a soluble element, but unlike Li, it is more readily incorporated into early forming carbonate and borate minerals during evaporation. Carbonate and many borate minerals preferentially incorporate B in tetrahedral coordination, which is enriched in ^{10}B [14–17]. If these minerals later dissolve, they decrease the water's δ^{11}B, assuming that water was isotopically similar to the water from which they originally precipitated [13]. Sr isotopes are included to address the role of lithology. Furthermore, our inclusion of data from the wells within the alluvial fan aims to further our understanding of solute fluxes to the Salar.

1.1. Background to the Salar de Atacama

The Salar de Atacama, the largest salt pan in Chile, lies between two first-order morphostructural units, the Western Cordillera to the east, and the Domeyko Range to the west. It interrupts the western slope of the Andes that is 200 km east of the Pacific coastline. The salar has a surface area of 3000 km^2 and estimates of the halite volume range between 1500 and 2200 km^3 [18–20]. Below the halite body is 600 m of claystone with minor sand [20], forming a very low permeability layer. Best estimates indicate that the halite unit in the salar started to accumulate within the last 10 Myr [21]. While the halite was accumulating, the relief between the salar and the Andean crest increased 2300 ± 1050 m [22]. Dated ignimbrites within the halite body indicate that the amount of salt has not increased uniformly during this time [21]. Between the Atana and Tucúcaro–Patao ignimbrites (4.0 to 3.1 Ma), 400 m of salt accumulated, followed by a hiatus of some 1–2 Myr, depending on the location within the salar. Salt accumulation resumed, but at much higher rates, especially during the deposition of the uppermost 200 m [21,23]. These accumulation changes are roughly consistent with the paleoclimate history of the area, with semi-arid to arid conditions occurring in the late Miocene–Pliocene before switching to being hyper arid [24–27] when salt deposition was most rapid. Coincident changes in relief, climate and salt accumulation suggest they may be linked to drainage, either in terms of drainage basin size, water fluxes and/or solute fluxes if the solute concentration has changed through time.

The salar's drainage basin extends beyond its topographic divide, how far is unknown [28], but it likely incorporates several basins that are topographically closed. Leakage of water from lakes within these basins has been proposed from geochemical constraints [29]. The salinity of this water may be elevated by evaporation or dissolution of mixed salt assemblages, so this water could already be enriched in elements such as Li and B before it reaches the Salar de Atacama. These sedimentary processes could overprint any increase in Li and B that is characteristic of water in hydrothermal systems [30].

Within the neighboring drainage system of the upper Loa river system, it was found that the impact of brine and evaporite dissolution on groundwater geochemistry was important in water draining

ignimbrite-covered areas ("Ignimbrite group"), but not in water that only drained stratovolcanoes along the Loa river ("Loa group") [13]. δ^7Li and Na/Li data for water entering the southeast part of the salar reported by Munk et al. [1], plot on a line whose δ^7Li and Na/Li was similar to the "Loa group" but not the "Ignimbrite" group, even though the eastern flanks of the salar are draped by the thick and extensive ignimbrites of the Miocene–Pliocene age. While some of the ignimbrites are shared between basins, this difference could indicate geochemical and isotopic heterogeneity of ignimbrites or the basement they obscure. Morphologically, though, the two basins differ. For this study, we sampled groundwater flowing towards the halite nucleus through the alluvial fan on the eastern border of the salar from wells and springs. The analysis of chemical and isotopic signatures was undertaken to address the role of warm or cold temperature weathering, brine leakage or salt dissolution on inflow water compositions.

1.2. Hydrological Description of the Salar de Atacama Basin

The region around Salar de Atacama has been arid or hyper arid since the end of the middle Miocene [31]. The streams that flow into the salar are groundwater fed and groundwater enters the salar directly. The inflow of water to the salar is from the Andes to the east and is negligible from the west [9]. Salt precipitates in the salar continuously, from shallow saline groundwater during dry periods and saline lakes when they were present during wet periods [23]. The continuous accumulation of salt has recorded the movement of a N-NW-striking reverse blind fault in the southern part of the salar, which has developed an offset of 900 m on its eastern side since the Pliocene [21,23]. Faults that may be linked to this Salar Fault extend beyond the boundary of the halite nucleus into the Tilocalar Valley and Cordón de Lila in the south, and along Cordillera de la Sal, Llano de la Paciencia and Cordillera Domeyko in the north [18,20]. Jordan et al. [21,32] hypothesized that the Salar Fault probably acted as a barrier to sub-horizontal groundwater flow, either due to contrastingly low permeability of the rocks to its west, or because halite at the fault zone impedes horizontal flow and promotes vertical flow. Maps [1] show abrupt increases in Li concentrations occur immediately west of the Salar Fault, especially between the fault and the northern portion of the Cordon de Lila. A second set of reverse faults, the Peine Fault system strikes N-NE with less displacement along the eastern side of the salar [20,21]. These faults may also influence groundwater flow based on a series of pools and surface drainage that align with its position based on seismic lines [21].

La Pacana caldera, the source of the rhyolitic Toconao ignimbrite (5–4 Ma) and the cogenetic and voluminous (>2000 km^3) dacitic Atana ignimbrite (4 Ma) [33,34] lies immediately east of the salar. The caldera is ~60 km N–S and ~35 km E–W and covers a N–S range that extends from the northern end of the salar to the southern third of the halite nucleus. Volcanism continued for at least an additional 2 Myr, producing dacite domes and younger ignimbrites in the southern half of the caldera depression. To the west and south of the caldera rim are young andesitic volcanic centers, including the active volcano Lascar. The slope between these young volcanoes and the salar is covered by ignimbrites and alluvial fans. These fans and ignimbrites, if they are fractured, act as aquifers that recharge at the western crest of the Andes and possibly further east. In the southeast part of the salar, where the exposed pre-volcanic Peine block separates the salar from the volcanic arc, groundwater flow is deflected from simple E to W to S to N. The Quebrada de Nacimiento Fault, which bounds the Peine block to its east, also acts as a barrier to flow, causing water to be retained in the lagoons of Miscanti and Miñiques. Large volumes of water flow into the salar's SE corner from the southern Monturaqui–Negrillar–Tilopozo (MNT) aquifer system through the Tilocalar Valley [1,35]. Water enters the MNT aquifer from the east, where it is postulated that shallow groundwater acquires salinity from salars to the east, and then flows close to the northern edge of Volcan Socompa where additional water enters the aquifer that has been modified by hydrothermal activity [35]. Further hydrothermal interactions might occur in the vicinity of the Tilocalar scoria cone.

2. Samples and Methods

Samples were collected using in situ submersible pumps from six wells located to the east of the salar margin (Figure 1, Table 1) or directly from springs and streams. All samples were filtered to < 0.4 µm in the field and stored in new, acid-cleaned polyethylene bottles. Samples were acidified to pH < 2 with nitric acid. Temperature and pH were measured in the field, and alkalinity on the same day by acid titration. Additional trace metal cations were measured at Rutgers University, using a Thermo iCAP-Q at Rutgers University with a Teflon introduction system and trace HF in the carrier acid to rinse out B. Concentrations were determined using synthetic standard mixtures and their accuracy checked with certified standards and seawater. Accuracy was typically better than 5% and the relative standard deviation typically 1–3%.

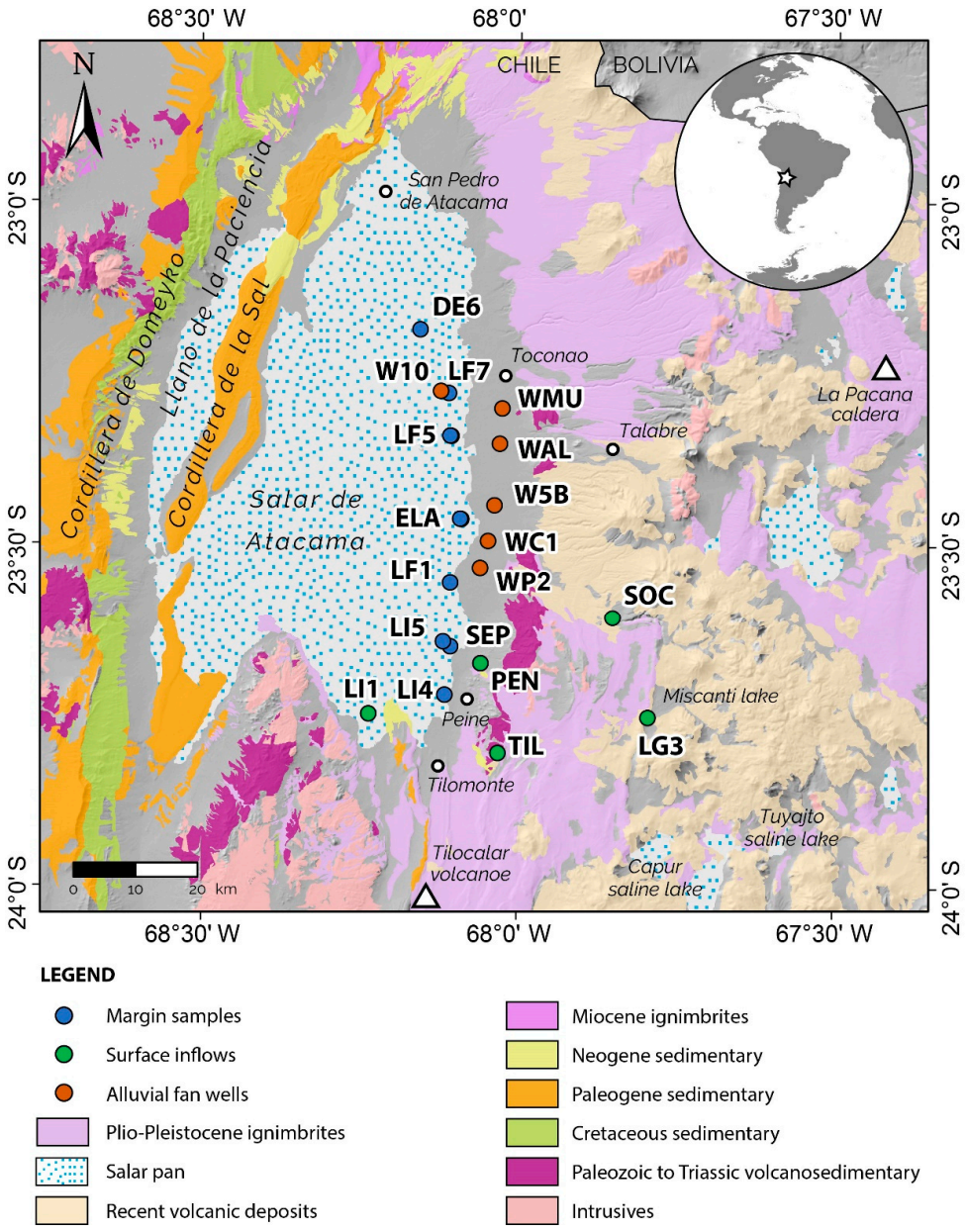

Figure 1. Map of the Salar de Atacama basin from References [36–38], showing the major rock units and the sample locations.

Table 1. Field measurements, concentration and isotopic data for water samples from the southern part of the Salar de Atacama.

	TDS g/L (g/L)	pH	alk (mg/L)	Cl (mg/L)	Br (mg/L)	SO_4 (mg/L)	Ca (mg/L)	K (mg/L)	Mg (mg/L)	Na (mg/L)	Sr (mg/L)	$^{87}Sr/^{86}Sr$	Li (mg/L)	δ^7Li	B (mg/L)	$\delta^{11}B$
Margin samples																
DE6	14.60	8.17	2.95	9500	2.54	3000	840	505	570	5200	21.6	0.71171	41.0	3.7	12.0	−9.2
LF7	0.66	8.08	5.07	224	0.19	148	38.3	23.5	11.6	227	0.5		10.1	5.5	10.6	−9.3
LF5	1.49	8.25	8.28	519	0.63	299	30.9	44.9	19.2	568	0.2	0.70866	1.6	6.9	31.2	−6.3
ELA	66.54	7.88	6.00	56000	7.7	6600	658	520	2400	31500	6.9	0.70787	428.0	5.6	30.1	−4.4
LF1	45.85	7.55	4.49	34884		3831	753	3326	1473	17820	7.6	0.70811	5.2	11.4	36.6	−6.8
SEP	9.32	8.29	3.05	6800	0.98	720	718	499	399	3700	12.5	0.70787	33.0	12.6	10.3	1.0
LI5	58.15	7.71	2.03	58710		5898	1843	4551	2373	29800	30.7	0.70794	251.6	11.5	81.9	−9.6
LI1	4.70	7.56	7.86	2491	1.09	1175	177	262	271	1830	2.7	0.70792	19.8	10.5	22.7	−3.5
Surface inflow																
HON	0.18	8.05	1.28	43	0.27	26	12	1	19	21	0.1	0.70864	0.3	6.5	4.0	2.7
PEN	2.40	7.36	2.46	1000	1.25	932	216	26	80	472	1.8	0.70767	1.3	9.2	5.9	6.1
TIL	3.02	7.04	2.75	1500	1.29	886	210	61	199	727	2.0	0.70750	2.2	8.8	7.0	6.8
LI4	3.61	7.32	5.21	2209	1.55	753	478	80.7	192	972	3.8	0.70792	3.0	6.8	11.5	6.4
SOC	0.77	8.64	4.23	128	0.29	314	19	10	44	103	0.3	0.70734	0.2	6.7	5.4	−0.1
LG3	7.57	8.68	1.95	2896	2.79	5024	673	368	303	3021	5.5	0.70715	2.6	10.6	51.8	4.0
Alluvial fan wells																
W10	0.59	8.02	3.34	228	0.15	100	10	27	23	180	0.3	0.70872	1.4	8.5	16.0	
WMU	0.95	7.14	4.48	381	0.487	212	25	31	31	315	0.6	0.70925	2.2	4.9	12.0	−5.1
WAL	2.49	8.91	2.80	395	3	1600	76	27	220	508	0.4	0.70740	0.7	9.1	10.7	0.4
W5B	6.10	6.56	9.59	4000	1.39	921	201	146	249	2400	1.8	0.70790	14.0	11.2	4.0	−1.4
WC1	1.67	9.86	16.13	366	0.61	265	4	18	28	580			3.1	10.5	18.9	−2.5
WP2	1.33	7.51	2.75	668	0.38	346	82	23	46	351	1.5	0.70850	2.5	10.4	5.0	2.4

Strontium isotopes were measured following chromatographic separation using AGW50x8 with hydrochloric acid. Samples were loaded on a Re filament with a Ta activator and analyzed using a VG Sector 54 thermal ionization mass spectrometer (TIMS) at Cornell University (Ithaca, NY, USA). Fractionation was corrected by normalizing to $^{86}Sr/^{88}Sr = 0.1194$. Measurement of NBS 987 was included with all analyses, and averaged 0.710245 ± 0.000006 (2, n = 40). Lithium isotopes were analyzed at Rutgers University (Piscataway, NJ, USA) using a ThermoScientific Neptune Plus MC-ICPMS following separation using two cation exchange columns (7 mL resin bed followed by 0.2 mL resin bed) filled with an AGW50 × 12 200−400 mesh and 0.5 N HCl as eluant. A sample of seawater was included with all sample batches and separated using different column pairs to ensure yields were quantitative. Lithium solutions of 20 ppb concentration were analyzed that, utilizing a Teledyne Cetac Aridus II and X-type Ni skimmer cone, yielded a signal exceeding 18 V on δ^7Li with an acid blank of < 150 mV. The high sensitivity of the instrument allows small samples to be processed though ion chromatography, which enables column calibrations to be stable. Standard–sample–standard (L-SVEC) bracketing was used, and signals matched to within 5%. A solution of IRMM-016 was included in each batch of analyses, and the long-term δ^7Li average of that and seawater were 0.1‰ ± 0.07 (2, n = 25) and +30.6‰ ± 0.12 (2, n = 18), respectively. Measurement of boron isotopes followed separation using a micro-sublimation technique [39]. Samples were run in duplicate and differed by less than 0.5‰. A seawater sample was included in every sublimation batch. Measurement of δ^{11}B was also made with the Thermo Neptune Plus at Rutgers University using a PFA micro-concentric spray chamber (ESI) and a 2% HNO_3 and 0.1% HF matrix. The signal intensity for δ^{11}B was about 350 mV for a 30 ppb solution, and the acid blank was < 2.5 mV. NIST 951 a was used for sample–standard bracketing. Solutions of the BAM standards AE120 and AE122, an acid blank and the seawater sample were run periodically throughout each analysis. Standards AE120 and AE122 yielded −19.9‰ ± 0.08 (2, n = 13) and +39.5‰ ± 0.14 (2, n = 13), respectively, and Sargasso seawater +40.3‰ ± 0.14 (n = 11).

3. Results

3.1. Elemental Characterization of Water

Data are reported in Table 1. The total dissolved solids (TDS) of well water in the alluvial margin is 1 to 6.1 g/L, so it can be characterized as slightly brackish. This is higher than in surface water, which ranges between 0.2 and 3.6 g/L [11,12]. Water has a near neutral pH or is alkaline, but the wells are more alkaline, with a pH reaching as high as 9.86 in WC1. Major cation and anion compositions of water sampled at the surface around the salar basin are shown in a Durov diagram (Figure 2).

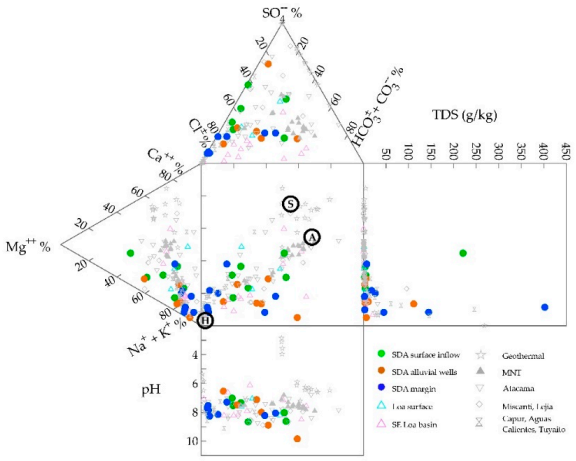

Figure 2. Durov figure including data from the Salar de Atacama (this study),the Loa groundwater basin [13], the Monturaqui-Negrillar-Tilopozo aquifer [35], neighboring basins Capur, Tuyaito and Aguas Calientes 3 [11], plus important regional thermal water [40,41].

3.2. Strontium Isotope Compositions

Almost all samples have $^{87}Sr/^{86}Sr$ ratios between 0.7075 and 0.7095, overlapping with the ignimbrite group from the Upper Loa basin [13]. In general, the northern catchment area of the salar has water with higher $^{87}Sr/^{86}Sr$ than the southern catchments [1], with water draining through the eastern alluvial fans having intermediate compositions. Of the wells, WMU, located between the Aguas Blancas and Talabre creeks, which originate on Lascar volcano, has the most radiogenic Sr. Its composition of 0.70925 is higher than the reported data for Lascar lava or ignimbrite (0.7056−0.7072; [42,43]) suggesting input of Sr from a more radiogenic source. One potential source are basement rocks, either Permo-Triassic volcanics or later-formed clastic units, such as the El Bordo unit [33,44], and exemplified by a single sample, DE6, with an $^{87}Sr/^{86}Sr$ composition of 0.71171. DE6 was collected north of the halite nucleus and coincident with the Peine Fault. Less radiogenic water in the more southerly wells is consistent with reported $^{87}Sr/^{86}Sr$ values for lavas and ignimbrites of the Cordón Punta Negra, as well as the Socompa and related groundwater(<0.7073 [35,42,43]). The brine in the salar, assuming it is recorded by evaporite minerals, has a composition of 0.7070 just north of the Cordón de Lila, around 0.7082 in the center, to 0.7086 just north of the halite nucleus [45] and indicates that inflow to the salar nucleus from radiogenic sources are more important in the northern portion of the basin.

3.3. Light Isotopes, Li and B

δ^7Li varies between +3.7‰ and +12.6‰ in streams and pools, and +4.9‰ and +11.2‰ in the springs and wells. Compared to samples from the Upper Loa basin [13], the samples reported here have higher δ^7Li for a given $^{87}Sr/^{86}Sr$ composition (Figure 3A). The springs at Peine and Tilomonte (PEN, TIL, LI1), wells W5B, WP2 and WAL, as well as margin sample SEP and ELA plot close to two streams sapping water from the Altiplano plateau [13]. Water entering the salar via the MNT aquifer, based on δ^7Li data [1] and $^{87}Sr/^{86}Sr$ data [35] probably plots close to the δ^7Li-$^{87}Sr/^{86}Sr$ trend defined by samples close to the San Pedro-Linzor line of volcanoes, and which formed the Ignimbrite group of samples in the Loa catchment [13] (Figure 3A). The brine in the Salar's southeast halite nucleus has a δ^7Li composition between +10 and +12‰ [1], which in combination with the Sr isotope data of salts [45] gives it the highest δ^7Li for its $^{87}Sr/^{86}Sr$ composition. This range is similar to nearby margin samples, such as SEP, but margin samples a little to the north, such as SEL, have considerably lower δ^7Li even though their $^{87}Sr/^{86}Sr$ is similar.

$\delta^{11}B$ varies between −5.2‰ to +2.5‰ in the wells, and the lowest $\delta^{11}B$ was recorded in WMU, which is close to the base of active volcano Lascar, whereas the highest was recorded in WP2. The range in $\delta^{11}B$ for the springs and streams, is −0.1 to +6.9‰. Wells, springs and streams lie on the same $\delta^{11}B$-$^{87}Sr/^{86}Sr$ trend as the groundwater and surface water of the Upper Loa drainage Basin (Figure 3B), where solute sources were attributed to ignimbrite and lava rock sources [13]. Except for a few samples located close to the halite nucleus, $\delta^{11}B$ values do not get as low as evaporite minerals in the area, which can have $\delta^{11}B$ below −10‰ [13,46].

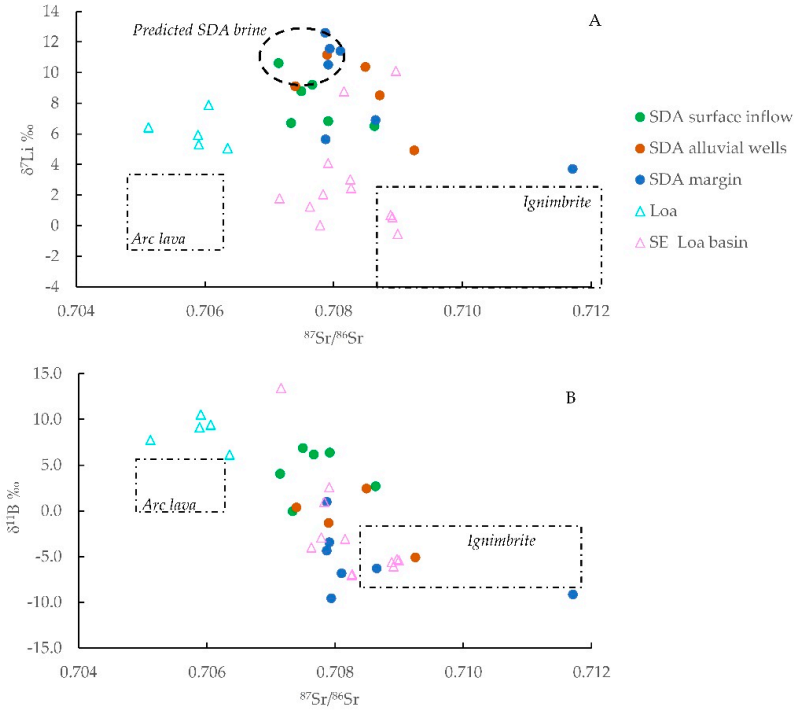

Figure 3. Diagrams showing the relationship between lithology, as indicated by $^{87}Sr/^{86}Sr$ and (**A**) Li and (**B**) isotopes. Ignimbrite and arc lava fields are from References [7,13,47,48]. Data for water in the neighboring upper Loa drainage basin is from [13], virtually the same. Ignimbrite and arc lava fields are from References [7,13,47,48].

4. Discussion

4.1. Chemical Constraints on Solute Fluxes

We identified two different trends and three endmembers (H, A and S; Figure 2). Figure 2 also includes regional hydrothermal water [40,41] and saline lake water from Capur and Tuyaito [11], lakes that could potentially leak into regional groundwater [29,30,49]. The two trends of Figure 2 share one endmember (H), which has high Na and Cl, indicating the likelihood of halite recycling and is similar in composition to saline lakes and El Tatio. In the adjacent upper Loa basin, the endmember for water draining ignimbrite-dominated areas (IG, [13]) is nearly coincident with (H). The other two endmembers have a greater proportion of Mg and Ca, but the trends are distinguished by the relative proportion of (HCO_3^- + CO_3^{2-}) and SO_4^{2-} (A, for alkaline, and S, for sulfate endmembers). These waters, in which sulfate increases, drain into the SE part of the salar but flow east of the Tilocalar valley in the Lomas de Quilvar. Samples from the steam-heated Apacheta geothermal site cluster at this endmember (S) [41]. The other trend, which comprises a larger number of samples, is defined by an increase in alkalinity. These waters, which plot furthest towards endmember (A), include the Río Talabre, the Río Jauna and groundwater in the Negrillar volcanic aquifer [11,35]. These three are all characterized by their proximity to young or active volcanoes: Lascar, the El Tatio volcanoes and Cerro Pular-Socompa. A spring close to geothermal site Torta de Tocorpuri, where Tassi et al. [41] proposed that limestone is the source for much of the CO_2, has a higher alkalinity than endmember (A). For comparison, both endmember water compositions in the upper part of the neighboring Loa basin, which drained stratovolcanoes or the Altiplano, plot close to (A) [13].

The data for the wells studied here either lie on trend (H)−(A) or are offset towards higher alkalinity but without an increase in Ca or Mg. WC1 has the most extreme Na-carbonate composition of the wells and based on location, wells WMU and W10 may be influenced by similar water. The high pH, Na concentration and alkalinity of WC1 indicate high CO_2 inputs and hydrolysis of Na-rich silicates. Similar compositions were reported for groundwater in Baja California, which had undergone

deep but rapid flow through fractured igneous and metamorphic rocks [50]. However, the high TDS of WC1 suggests a long residence time or higher weathering rates, possibly influenced by elevated temperatures. One reason that WC1, as well as WMU and W10 have compositions that are not typical of other water in the basin is they represent deeper groundwater, whereas other samples reported to date are for rivers and springs. While those are groundwater fed, it is likely that they are fed by very shallow groundwater or from perched aquifers, common in these volcanic systems where welded ignimbrites or lava provide confining layers [51].

4.2. Isotopic Approaches

The Li and B isotopic compositions of water are affected by the formation and interaction with secondary minerals, and fractionation is temperature dependent. The mineralogy of the host rocks on isotope composition is small in comparison. Lithium bonds via O and is either in tetrahedral or octahedral coordination, in water and minerals, and δ^7Li is favored in lower coordination number sites. When secondary minerals equilibrate with water, regardless of type, if there are octahedral sites for Li to occupy, a greater proportion of them are occupied by ^{6}Li. This leaves water enriched in δ^7Li [52]. The plot of δ^7Li versus ^{87}Sr/^{86}Sr (Figure 3A), which includes the fields for ignimbrite and lava [7,13,47,48], shows that the role of lithology from ^{87}Sr/^{86}Sr does not account for the variation in δ^7Li. Boron in water likewise becomes enriched in the heavy isotope, but the mechanism is different to that of Li. However, like Li, the role of lithology is minor unless marine limestone is involved, which has a high δ^{11}B compared to silicates [13]. Boron exists as $B(OH)_3$ and $B(OH)_4^-$ in water according to pH with an isotope separation around 20‰ at typical Earth surface temperatures [15,16]. Because $B(OH)_4^-$, which is enriched in ^{10}B, is the preferred B species incorporated into clays, water becomes enriched in δ^{11}B [14]. While boron isotopes reflect silicate weathering and clay formation there is a strong pH dependence. The isotope separation between the two isotopes of B does not change, but the isotope separation between bulk water and ($B(OH)_4^-$) increases as pH decreases. The low partition coefficient of $B(OH)_3$ into minerals causes B to behave in a more conservative fashion at a low pH and the formation of secondary minerals produces only small increases in the water's δ^{11}B. For example, there is a greater isotope expression for B uptake into secondary phases that occurs at pH 8.5 than at pH 7.5 because the K_d at pH 8.5 is 33 compared to 5, even though the equilibrium isotope separation between bulk water and $B(OH)_4^-$ at pH 8.5 is less [53]. Based on these factors that influence water's δ^7Li and δ^{11}B, we address the solute fluxes in the Salar de Atacama.

4.3. Saline Influxes to the Salar de Atacama

One explanation for the extraordinary enrichment of Li in the Salar de Atacama brine is water that has been enriched before it reaches the halite nucleus. It is possible that precipitation of salts in topographically closed but hydrologically open basins leaves Li in brine that drains into the regional groundwater [29]. As well as capturing brine from neighboring basins or meteoric water dissolving evaporites, water–rock reactions with dilute water or saline groundwater continuously extract Li.

High Cl/Br ratios as well as high Cl and Na concentrations are often used to demonstrate the presence of dissolved halite [54]. High Cl/Br ratios and low δ^{11}B were used to demonstrate the role for evaporite mineral dissolution in influencing the geochemistry of water draining ignimbrite covered areas of the neighboring upper Loa basin [13]. In order to evaluate the halite dissolution, we studied Na/B and Na/Li ratios compared to Cl/Br (Figure 4); B and Li concentrations are normalized to Na to address possible changes due to evaporative enrichment. In terms of B, corresponding increases in Na/B and Cl/Br (Figure 4A) are consistent with halite dissolution. In comparison to the upper Loa basin, Na/Li ratios do not change or slightly decrease (Figure 4B) as Cl/Br increases. Moreover, two samples near Toconao (HON and LF7) have remarkably low Na/Li. If increasing Cl/Br ratios indicate halite is a source of Cl, and hence Na, either Li and halite come from the source area but Li does not itself originate from halite, or the halite itself is extremely enriched in Li, possibly due to Li-rich inclusions since Li does not fit into the halite lattice. The sodium-normalized distribution coefficients

of Li in halite are around 0.05 to 0.005 [5], so if Cl/Br and Li only increase due to dissolving halite, the brine from which that halite precipitated must have had a very high Li concentration.

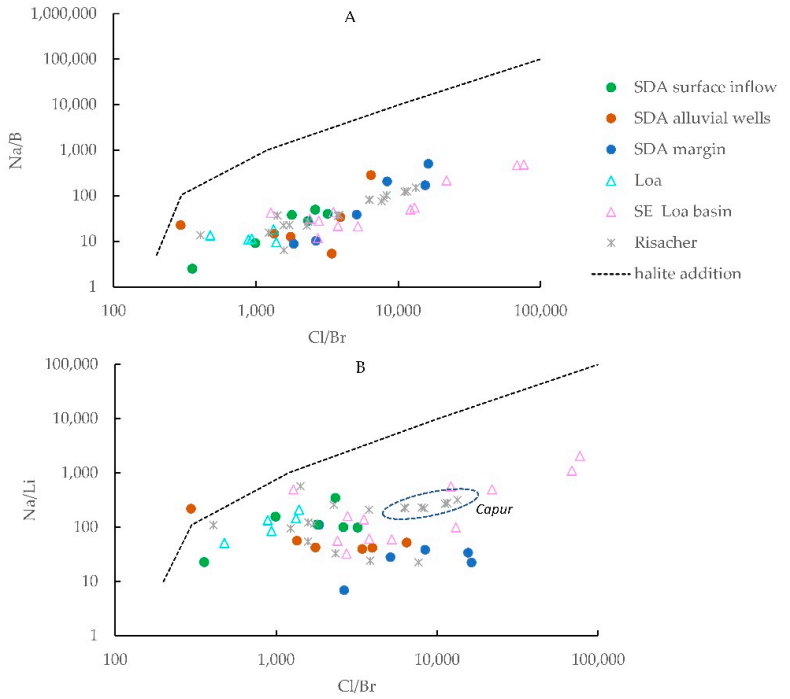

Figure 4. Diagrams showing the relationship between Na/B and Cl/Br (**A**), and Na/Li and Cl/Br (**B**). The dotted line indicates the effect that evaporate dissolution, primarily halite, has on water compositions. The effect on B is shown in (**A**) and (**B**).

Boron isotopes in the Upper Loa drainage basin did not conform to open or Rayleigh isotope fractionation models [13] for two reasons. First, evaporite minerals, in which B often occurs as $B(OH)_4^-$, are enriched in ^{10}B and their dissolution imparts a negative $\delta^{11}B$ signature relative to the original water [13,17], so mixing was more important. Second, pH was not so high that B would be taken up by clays compared to the amount released from silicates. Unlike the southern ignimbrite covered part of the upper Loa drainage basin, there is no indication from $\delta^{11}B$ that substantial quantities of evaporite minerals dissolve except within the salar's margin and at WMU. This is consistent with the idea that buried salts formed within ancient salt lakes would have been long exhausted within aquifer catchments since there are no salars of sufficient size where evaporites could persist to influence modern ground water [35,49]. In basins such as Capur or Tuyaito there is also a conspicuous absence of large accumulations of salt [51]. Li-rich sedimentary salts as a Li source can be discounted using $\delta^{11}B$.

4.4. Rock Weathering Sources: Insights from δ^7Li and $\delta^{11}B$

Models describing mixing, open system and Rayleigh fractionation, used to describe stable isotopes in rivers draining volcanic systems, including water in the upper Loa basin [13], are applied here. The same equations are used to address Li and B; the example given is for Li [55]. Open system fractionation follows $\delta^7Li_w = \delta^7Li_i - (1 - f)$. $\Delta^7Li_{c\text{-}w}$ and Rayleigh fractionation $\delta^7Li_w = \delta^7Li_i - \Delta^7Li_{c\text{-}w}.\ln(f)$, where δ^7Li_w is the isotope composition of the evolving water, δ^7Li_i its initial isotope composition, $\Delta_{c\text{-}w}$ the isotope separation between clay and f the fraction of Li remaining in solution. Li was normalized to Na, and Na was assumed to be conservative.

Around the Salar de Atacama, pH gets sufficiently high in some of the wells to allow fractionation during secondary mineral formation to be apparent. Wells WAL and WC1 have a pH around 9 or above, suggesting a fractionation factor between water and clay of around 0.988 [14]. Applying open system fractionation using this fractionation factor and an initial water composition of WMU, which is

also like El Tatio [13], produces a curve around which these two samples plot (Figure 5A). WP2 also plots close to this line although its pH is close to neutral, but its B isotope composition could have been set earlier where pH was high. Spring water at Peine and Tilomonte (PEN, TIL) have higher $\delta^{11}B$ than the line describing the batch model evolution of groundwater but have compositions consistent with a fractionation factor of 0.985 and adsorption at a lower pH. The cause of the enrichment in the Socaire (SOC), the Honor (HON), margin sample LF7 as well as the Loa streams is currently unknown.

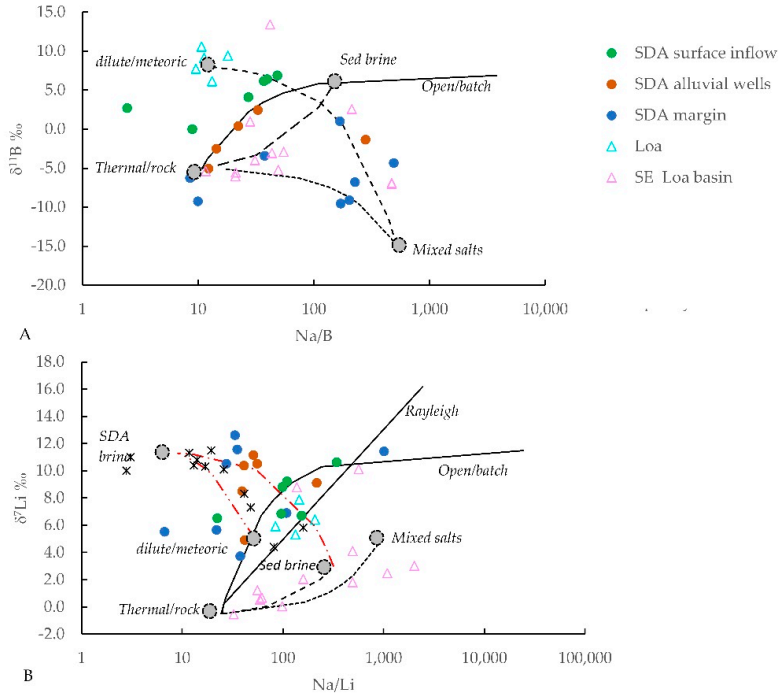

Figure 5. Diagrams showing the relationship between $\delta^{11}B$ and Na/B (**A**), and $\delta^{7}Li$ and Na/Li (**B**). Solid lines represent isotope fractionation following Rayleigh or batch (open) models for partitioning between solution and secondary minerals. Dashed lines represent mixing between different end-member reservoirs (filled gray circles).

Lithium isotopes, unlike B's, are not influenced by evaporite mineral dissolution because Li is not incorporated into evaporites. Open and closed fractionation in the upper Loa system were modeled using an initial $\delta^{7}Li$ value of water, the same as rock and El Tatio hydrothermal water. Using an isotope separation between water and clay, a $\Delta^{7}Li_{c\text{-}w}$ of −3.5‰ produced $\delta^{7}Li$ values and Li/Na ratios close to the measured surface water. This value is low for describing Li in octahedral sites but reasonable for surface adsorption or uptake by kaolinite [56,57]. The same $\Delta^{7}Li_{c\text{-}w}$ value was applied to groundwater following open system fractionation, which accounts for the importance of Li release from rocks and not just the removal processes during clay formation (Figure 5B).

Samples from the southeastern section of the Salar de Atacama do not plot with the ignimbrite group of samples from the upper Loa Basin, even though the area is also covered by ignimbrites (Figure 1). Groundwater emanating at the Peine and Tilomonte springs (PEN, TIL) have more evolved compositions in terms of Li isotopes than nearby surface water, such as Socaire (SOC) or saline water in Capur or Tuyaito, but is not as evolved isotopically as brine in the southeast part of the salar. Since rock dissolution dampens the increase in $\delta^{7}Li$ in the direction of flow for groundwater [58], the high $\delta^{7}Li$ of the groundwater at PEN and TIL relative to the nearby Socaire (SOC) stream suggest either a long residence time of water in the aquifer, or water had been at the surface before it entered the aquifer, for example, in a lake. For the highest $\delta^{7}Li$ to occur in the salar is consistent with it being the end of the regional flow paths. The high $\delta^{7}Li$ of Miscanti lake (LG3) suggests that this lake also represents the end of its catchment and does not leak water. In comparison, saline water in the topographically

closed basins Capur and Tuyaito do not have as high δ^7Li [46], and they are likely to be locations where infiltration into the regional groundwater system occurs.

Changes in the δ^7Li-Na/Li of inflow at the northern end of the Tilocalar valley was explained by Li isotope fraction and removal to secondary minerals during evaporative enrichment [1]. The brine in the nucleus of the salar is extremely enriched in Li relative to Na, and even a minor fraction of this brine will significantly change the composition of water it may mix with. Consequently, any sample located close to the salar could have its Li content affected by the nucleus brine. Most of the freshwater wells in the alluvial fans lie close to a mixing line between the salar brine and freshwater inputs, especially those further to the south. Given the depth of these wells (90 to 180 m), the extent of the density-driven mixing appears to laterally extend 5–10 km east of the limit of the halite nucleus surface [59]. Although the PEN and TIL springs also lie on this mixing line, the nucleus brine cannot influence them as they sit above the salar. However, if $\Delta^7Li_{c\text{-}w}$ is increased to −12‰ (= 0.988), open system fractionation accounts for the composition of both the PEN and TIL springs as well as well water at WMU and WAL, and some of the water in the Loa basin such as the V. Barro and Silala streams [13]. This fractionation factor is consistent with a temperature of 80 °C [57], reasonable for deep groundwater in this volcanically active area. However, the increase in Li with Cl for samples at a higher elevation than the salar requires some explanation, as do the very low Na/Li of the Honor stream and nearby LF7 sample. This is addressed next.

4.5. A Volcanic Origin of Li

Changes in Cl/Br and Na/Li (and Cl/Br-Li) indicate there is a Li- and Cl-rich, Br- and B-poor source that cannot be the salar brine because it affects water above the salar. Furthermore, this source affects different parts of the salar-the area near the Tilocalar valley and around Toconao–where the most dilute water was sampled.

Li's increase with Cl/Br [48] suggest it is transported with Cl–rich water towards the Salar de Atacama, but δ^{11}B indicates it is not with water that acquired salinity from sedimentary halite. This differs from the situation in the neighboring upper Loa basin where δ^7Li and δ^{11}B were consistent with drainage from a system that had contained brine and salt. The formation of the regions multiple and large calderas that occurred during the Miocene–Pliocene ignimbrite flareup, when the climate was dry, provides a clue. Any brine or evaporite sequence that formed in one of the caldera lakes during their active stages, including La Pacana, would be Li-rich. Volcanism can explain the overall enrichment of Li in the salty water of the region, but does it account for the exceptional qualities of the Salar de Atacama?

Magnetotelluric surveys indicate low electrical resistivity zones occur a few km below volcanic edifices, including volcanoes in the central Andes [60,61]. Models indicate that these zones represent a brine lens from which a halite cap precipitates. The depth of the low resistivity zone indicative of saline fluids and hydrothermal activity under Lascar and Salar de Aguas Calientes is around 1 km. A deeper (up to 6 km) conductive layer to the south of Lascar is indicative of either fluids or a magma chamber [60]. The depth of the upper conductive layer is similar to the topographic difference between the ignimbrite plateau on which the volcanoes of the western Cordillera sit, and the modern salar surface, meaning that the upper conductive layer is close in elevation to the salar surface. Shallow magma chambers and the massive Altiplano–Puna magmatic body cool by radiation, but also by convection of groundwater. We postulate that groundwater close to the Salar de Atacama is involved in hydrothermal reactions of rock and gets close to where Li-, B- and Br-rich vapor phases partitioned from a volcanic brine [62] or even a volcanic halite cap may dissolve into it. The steep eastern slope and unique position of the Salar de Atacama relative to the Andean crest allows this groundwater mix into shallow, meteoric dominated groundwater. The low Na/Li and Na/B in WMU, HON and LF7 indicate the possibility of small traces of a volcanic vapor, probably from Lascar, reaching shallow levels in the crust, although the δ^7Li is low compared to basalt measurements of magmatic fluids overlying the subducting slabs [52]. However, the reaction with wall rocks, which happens if ignimbrites or

the basement have low δ^7Li [7], could lower this higher slab value. The higher Na/Li and lower δ^7Li of samples in the Tilocalar area suggest a source that was made more saline by surface brine interacting with a hydrothermal system associated with the historically active Socompa volcano or with the Tilocalar cone.

According to established basin flow models [63], the topographic hole in which the salar sits focusses flow of deep and intermediate-depth groundwater towards it, transporting Li. As the elevation difference on the eastern side of the salar increased following the peak of the ignimbrite flare-up, so the increase in salt accumulation indicates redistribution of salt and brine to the salar. A partly magmatic origin of Li is not dissimilar to models already proposed based on melt inclusions [64,65]. In the ignimbrites of La Pacana, reported Li concentrations in melt inclusions do, albeit rarely, exceed 1000 ppm, although we point out that many ignimbrites are dacitic, not rhyolitic [66]. These melt inclusions are less enriched than those in intracontinental systems studied in North America [64,65]. For the Salar de Atacama, eruption of volcanic products and their subsequent weathering is not required to bring volcanic Li to the surface−topography does this instead. A second possibility, though one currently not supported by observations in northern Chile, is that there are clays with very high Li enrichments within these nearby calderas. Diagenesis involving water enriched by magmatic fluids in a manner that created the Li-rich clays of the McDermitt system is one scenario ([67], this volume). Li-illite minerals occur in sediments of the Guayatayoc playa lake located at the eastern cordillera of the Andes, and although considered detrital [6], could be similar to the clay described in the McDermitt caldera's Thacker Pass deposit [67]. Passage of groundwater through these buried clays leaches and transports Li to the salar.

5. Conclusions

Groundwater reaching the salar have spatially varied and distinct chemical signatures due to complex topography and structures. Low δ^7Li values in water draining the area with active or dormant volcanoes are consistent with water–rock reactions occurring at somewhat elevated temperatures due to a high geothermal gradient or associated hydrothermal systems. In other aquifers, such as those in the Lomas de Quilvar, water has a high δ^7Li, which can be explained by a longer subsurface residence time. A fraction of the water in the Lomas de Quilvar aquifers leaked through lake bottoms within the topographically closed basins of the Altiplano. This water does not carry a B isotope signature of evaporite mineral dissolution and supports earlier models that salinity is derived from evaporated water and not from dissolution of buried salts. The highest δ^7Li compositions occur in the Salar de Atacama brine, the end of the groundwater flow.

There are two likely reasons why Li concentrations of the Salar de Atacama brine are so high even compared to other closed basins within the Li-triangle of the central Andes: First, silicate weathering under conditions of regionally elevated temperatures aids in the effective leaching of Li from the extensive ignimbrites and other volcanic rocks although the rocks themselves are not exceptionally enriched in Li; and second, the proximity to active volcanoes and a huge magmatic body, whose cooling drives large-scale groundwater convection, combined with the fact that more than 1000 m of elevation adjacent to the salar allows fluids, which would normally remain at depth, to reach the surface where they then evaporate in the salar.

Author Contributions: Conceptualization, L.G.; software, L.G.; resources, F.Á.-A.; writing—Original draft, L.G., and F.Á.-A. All authors have read and agreed to the published version of the manuscript.

Funding: This research was funded by NSF grants ATM-9631291, ATM-9709786, FONDECYT grant 11160325 and MSI through the grant Millennium Nucleus for Metal Tracing along Subduction.

Acknowledgments: We would like to thank Teresa Jordan for invaluable conversations regarding the structure of the Salar de Atacama basin. LVG would like to acknowledge the help and support of SQM for this work.

Conflicts of Interest: The authors declare no conflict of interest.

References

1. Munk, L.A.; Boutt, D.F.; Hyneck, S.; Moran, B. Hydrogeochemical fluxes and processes contributing to the formation of lithium-enriched brines in a hyper-arid continental basin. *Chem. Geol.* **2018**, *493*, 37–57. [CrossRef]
2. Munk, L.A.; Hynek, S.A.; Bradley, D.; Boutt, D.F.; Labay, K.; Jochens, H. Lithium brines: A global perspective. *Rev. Econ. Geol.* **2016**, *18*, 339–365.
3. López Steinmetz, R.L.; Salvi, S.; García, M.G.; Peralta Arnold, Y.; Béziat, D.; Franco, G.; Constantitni, O.; Córdoba, F.; Caffe, P.J. Northern Puna Plateau-scale survey of Li brine-type deposits in the Andes of NW Argentina. *J. Geochem. Explor.* **2018**, *190*, 26–38. [CrossRef]
4. Ide, Y.F.; Kunasz, I.A. Origin of Lithium in Salar de Atacama, Northern Chile. Geology of the Andes and Its Relation to Hydrocarbon and Mineral Resources: Houston, Texas, Circum-Pacific Council for Energy and Mineral Resources. *Earth Sci. Ser.* **1989**, *11*, 165–172.
5. Godfrey, L.V.; Chan, L.H.; Alonso, R.N.; Lowenstein, T.K.; McDonough, W.F.; Houston, J.; Li, J.; Bobst, A.; Jordan, T.E. The role of climate in the accumulation of lithium-rich brine in the central Andes. *Appl. Geochem.* **2013**, *38*, 92–102. [CrossRef]
6. López Steinmetz, R.L. Lithium- and boron-bearing brines in the Central Andes: Exploring hydrofacies on the eastern Puna plateau between 23° and 23°30′S. *Miner. Depos.* **2017**, *52*, 35–50.
7. Meixner, A.; Sarchi, C.; Ludassen, F.; Becchio, R.; Caffe Pj Lindsay, J.; Rosner, M.; Kasemann, S.A. Lithium concentrations and isotope signatures of Palaeozoic basement rocks and Cenozoic volcanic rocks from the Central Andean arc and back-arc. *Miner. Depos.* **2019**, 1–14. [CrossRef]
8. Garcia, M.G.; Borda, L.G.; Godfrey, L.V.; López Steinmetz, R.L.; Losada-Calderon, A. Characterization of lithium cycling in the Salar De Olaroz, Central Andes, using a geochemical and isotopic approach. *Chem. Geol.* **2019**, *531*, 119340. [CrossRef]
9. DGA-CORFO-ONU-CCC. *Investigacion de Recursos Hidraulicos en el Norte Grande*; CHI-535; CORFO: Santiago, Cihle, 1977; 55p.
10. Moraga, B.A. Estudio geologico del Salar de Atacama, Provincia de Antofagasta. *Inst. Inv. Geol. Bol.* **1974**, *29*, 56.
11. Risacher, F.; Alonso, H.; Salazar, C. *Geoquímica de aguas en cuencas cerradas, I, II, III Regiones, Chile*; Technical Report S.I.T. n 51; Ministerio de Obras Públicas, Dirección General de Aguas: Santiago, Chile; Available online: http://horizon.documentation.ird.fr/exl-doc/pleins_textes/pleins_textes_7/divers2/010019475.pdf (accessed on 24 February 2020).
12. Boschetti, T.; Cortecci, G.; Barbieri, M.; Mussi, M. New and past geochemical data on fresh to brine waters of the Salar de Atacama and Andean Altiplano, northern Chile. *Geofluids* **2007**, *7*, 33–50. [CrossRef]
13. Godfrey, L.V.; Herrera, C.; Gamboa, C.; Mathur, R. Chemical and isotopic evolution of groundwater through the active Andean arc of Northern Chile. *Chem. Geol.* **2019**, *518*, 32–44. [CrossRef]
14. Palmer, M.R.; Spivack, A.; Edmond, J.M. Temperature and pH controls over isotopic fractionation during adsorption of boron on marine clay. *Geochim. Cosmochim. Acta* **1987**, *51*, 2319–2323. [CrossRef]
15. Oi, T.; Nomura, M.; Musashi, M.; Ossaka, T.; Okamoto, M.; Kakihana, H. Boron isotopic composition of some boron minerals. *Geochim. Cosmochim. Acta* **1989**, *53*, 3189–3195. [CrossRef]
16. Oi, T.; Kato, J.; Ossaka, T.; Kakihana, H. Boron isotope fractionation accompanying boron mineral formation from aqueous boric acid–sodium hydroxide solutions at 25 °C. *Geochem. J.* **1991**, *25*, 377–385. [CrossRef]
17. Palmer, M.R.; Helvaci, C. The boron isotope geochemistry of the Neogene borate deposits of Western Turkey. *Geochim. Cosmochim. Acta* **1997**, *61*, 3161–3169. [CrossRef]
18. Muñoz, N.; Charrier, G.R.; Jordan, T.E. Interactions between basement and cover during the evolution of the Salar de Atacama Basin, northern Chile. *Revista Geológica de Chile* **2002**, *29*, 55–80. [CrossRef]
19. Pananont, P.; Mpodozis, C.; Blanco, N.; Jordan, T.E.; Brown, L.D. Tectonic Evolution of the Northwest Salar de Atacama Basin, Northern Chile. *Tectonics* **2004**. [CrossRef]
20. Jordan, T.E.; Mpodozis, C.; Muñoz, N.; Blanco, N.; Pananont, P.; Gardeweg, M. Cenozoic subsurface stratigraphy and structure of the Salar de Atacama Basin, northern Chile. *J. S. Am. Earth Sci.* **2007**, *23*, 122–146. [CrossRef]
21. Jordan, T.E.; Muñoz, N.; Hein, M.; Lowenstein, T.; Godfrey, L.; Yu, J. Active faulting and folding without topographic expression in an evaporite basin, Chile. *GSA Bull.* **2002**, *114*, 1406–1421. [CrossRef]

22. Jordan, T.E.; Nester, P.L.; Blanco, N.; Hoke, G.D.; Dávila, F.; Tomlinson, A.J. Uplift of the Altiplano-Puna Plateau: A view from the west. *Tectonics* **2010**, *29*, TC5007. [CrossRef]
23. Lowenstein, T.K.; Hein, M.C.; Bobst, A.L.; Jordan, T.E.; Ku, T.L.; Luo, S. An assessment of stratigraphic completeness in climate-sensitive closed-basin lake sediments: Salar de Atacama, Chile. *J. Sediment. Res.* **2003**, *73*, 91–104. [CrossRef]
24. Sáez, A.; Cabrera, L.; Garcés, M.; Bogaard, P.; Jensen, A.; Gimeno, D. The stratigraphic record of changing hyperaridity in the Atacama Desert over the last 10 Ma. *Earth Planet. Sci. Lett.* **2012**, *355*, 32–38. [CrossRef]
25. Jordan, T.; Kirk-Lawlor, N.E.; Blanco, P.N.; Rech, J.A.; Cosentino, N.J. Landscape modifications in response to repeated onset of hyperarid paleoclimate states since 14 Ma, Atacama Desert, Chile. *Geol. Soc. Am. Bull.* **2014**, *126*, 1016–1046. [CrossRef]
26. Evanstar, L.A.; Hartley, A.J.; Archert, S.G.; Neilson, J.E. Climatic and halokinetic controls on alluvial-lacustrine sedimentation during compressional deformation, Andean forearc, northern Chile. *Basin Res.* **2015**, 1–24. [CrossRef]
27. de Wet, C.B.; Godfrey, L.; de Wet, A.P. Sedimentology and stable isotopes from a lacustrine-to-palustrine limestone deposited in an arid setting, climatic and tectonic factors: Miocene-Pliocene Opache Formation, Atacama Desert, Chile. *Palaeogeogr. Palaeoclim. Palaeoecol.* **2015**, *426*, 46–67. [CrossRef]
28. Corenthal, L.G.; Boutt, D.F.; Hynek, S.A.; Munk, L.A. Regional groundwater flow and accumulation of a massive evaporite deposit at the margin of the Chilean Altiplano. *Geophys. Res. Lett.* **2016**, *43*, 8017–8025. [CrossRef]
29. Risacher, F.; Alonso, H.; Salazar, C. The origin of brines and salts in Chilean salars: A hydrochemical review. *Earth Sci. Rev.* **2003**, *63*, 249–293. [CrossRef]
30. Risacher, F.; Fritz, B.; Hauser, A. Origin of components in Chilean thermal waters. *J. S. Am. Earth Sci.* **2011**, *31*, 153–170. [CrossRef]
31. Rech, J.A.; Currie, B.S.; Michalski, G.; Cowan, A.M. Neogene climate change and uplift in the Atacama Desert, Chile. *Geology* **2006**, *34*, 761–764. [CrossRef]
32. Jordan, T.E.; Godfrey, L.V.; Munoz, N.; Alonso, R.N.; Lowenstein, T.L.; Hoke, G.; Peranginangin, N.; Isacks, B.L.; Cathles, L. Orogenic-scale ground water circulation in the Central Andes: Evidence and consequences. In Proceedings of the 5th ISAG (International Symposium on Andean Geodynamics), Toulouse, France, 16–18 September 2002; Institut de Recherche pour le Développement, Universite´ Paul Sabatier: Toulouse, France, 2002; pp. 331–334.
33. Gardeweg, M.; Ramírez, C.F. La Pacana caldera and the Atana Ignimbrite—A major ash-flow and resurgent caldera complex in the Andes of northern Chile. *Bull. Volcanol.* **1987**, *49*, 547–566. [CrossRef]
34. Lindsay, J.M.; de Silva, S.; Trumbull, R.; Emmermann, R.; Wemmer, K.; La Pacana caldera, N. Chile: A re-evaluation of the stratigraphy and volcanology of one of the world's largest resurgent calderas. *J. Volcanol. Geotherm. Res.* **2001**, *106*, 145–173. [CrossRef]
35. Rissmann, C.; Leybourne, M.; Benn, C.; Christenson, B. The origin of solutes within the groundwaters of a high Andean aquifer. *Chem. Geol.* **2015**, *396*, 164–181. [CrossRef]
36. Marinovic, N.; Lahsen, A. *Hoja Calama: Región de Antofagasta, escala 1:250.000, Santiago, Carta Geológica de Chile, Serie Geología Básica 58*; Instituto de Investigaciones Geológicas: Santiago, Chile, 1984; p. 140.
37. Ramírez, C.; Gardeweg, M. *Geología de la hoja Toconao: Región de Antofagasta, escala 1:250.000, Santiago, Carta Geológica de Chile, Serie Geología Básica 54*; Instituto de Investigaciones Geológicas: Santiago, Chile, 1982; p. 122.
38. Becerra, J.; Henríquez, S.; Arriagada, C. Geología del área Salar de Atacama, región de Antofagasta, Escala 1:100.000, Santiago, Carta Geológica de Chile, Serie Geología Básica 166. *Serv. Natl. Geol. Miner.* **2014**, *1*, 46.
39. Wang, B.S.; You, C.F.; Huang, K.F.; Wu, S.F.; Aggarwal, S.K.; Chung, C.H.; Lin, P.Y. Direct separation of boron from Na- and Ca-rich matrices by sublimation for stable isotope measurement by MC-ICP-MS. *Talanta* **2010**, *82*, 1378–1384. [CrossRef]
40. Cortecci, G.; Boschetti, T.; Mussi, M.; Herrera Lameli, C.; Mucchino, C.; Barbieri, M. New chemical and original isotopic data on waters from El Tatio geothermal field, northern Chile. *Geochem. J.* **2005**, *39*, 547–571. [CrossRef]
41. Tassi, F.; Aguilera, F.; Darrah, T.; Vaselli, O.; Capaccioni, B.; Poreda, R.J.; Delgado Huertas, A. Fluid geochemistry of hydrothermal systems in the Arica–Parinacota, Tarapacá and Antofagasta regions (northern Chile). *J. Volcanol. Geotherm. Res.* **2010**, *192*, 1–15. [CrossRef]

42. Harmon, R.S.; Barreiro, B.A.; Moorbath, S.; Hoefs, J.; Francis, P.W.; Thorpe, R.S.; Déruelle, B.; McHugh, J.; Viglino, J.A. Regional O-, Sr-, and Pb-isotope relationships in late Cenozoic calc-alkaline lavas of the Andean Cordillera. *J. Geol. Soc.* **1984**, *141*, 803–822. [CrossRef]
43. Déruelle, B.; Figueroa, O.; Moorbath, S. Basalts of the Chilean Altiplano, south-central Andes. In Proceedings of the Third ISAG, St Malo, France, 17–19 September 1996; pp. 559–562.
44. Mpodozis, C.; Arriagada, C.; Basso, M.; Roperch, P.; Cobbold, P.; Reich, M. Late Mesozoic to Paleogene stratigraphy of the Salar de Atacama Basin, Antofagasta, northern Chile: Implications for the tectonic evolution of the central Andes. *Tectonophysics* **2005**, *399*, 125–154. [CrossRef]
45. Carmona, V.; Pueyo, J.J.; Taberner, C.; Chong, G.; Thirlwall, M. Solute inputs in the Salar de Atacama (N. Chile). *J. Geochem. Explor.* **2000**, *69–70*, 449–452. [CrossRef]
46. Lagos, L.V. Hidrogeoquímica de Fuentes Termales en Ambientes Salinos Relacionados con Salares en Los Andes del Norte de Chile. Master's Thesis, University of Chile, Santiago, Chile, 2017.
47. Rosner, M.; Erzinger, J.; Franz, G.; Trumbull, R. Slab-derived boron isotope signatures in arc volcanic rocks from the Central Andes and evidence for boron isotope fractionation during progressive slab dehydration. *Geochem. Geophys. Geosyst.* **2003**, *4*, 1–25. [CrossRef]
48. Kay, S.M.; Coira, B.L.; Café, P.J.; Chen, C.-H. Regional chemical diversity, crustal and mantle sources and evolution of central Andean Puna plateau ignimbrites. *J. Volcanol. Geotherm. Res.* **2010**, *198*, 81–111. [CrossRef]
49. Risacher, F.; Fritz, B. Origin of salts and brine evolution of Bolivian and Chilean salars. *Aquat. Geochem.* **2009**, *15*, 123–157. [CrossRef]
50. Ouysse, S.; Wehncke, E.V.; Carrillo Rivera, J.J. Investigating regional groundwater flow systems in baja california central desert region. *Int. J. Hydrol.* **2018**, *2*, 00057. [CrossRef]
51. Herrera, C.; Custodio, E.; Chong, G.; Lambán, L.J.; Riquelme, R.; Wilke, H.; Jódar, J.; Urrutia, J.; Urqueta, H.; Sarmiento, A.; et al. Groundwater flow in a closed basin with a saline shallow lake in a volcanic area: Laguna Tuyajto, northern Chilean Altiplano of the Andes. *Sci. Total Environ.* **2016**, *541*, 303–318. [CrossRef] [PubMed]
52. Penniston-Dorland, S.; Liu, X.-M.; Rudnick, R.L. Lithium isotope geochemistry. *Rev. Mineral. Geochem.* **2017**, *82*, 165–217. [CrossRef]
53. Rose, E.F.; Chaussidon, M.; France-Lanord, C. Fractionation of boron isotopes during erosion processes: The example of Himalayan rivers. *Geochim. Cosmochim. Acta* **2000**, *64*, 397–408. [CrossRef]
54. Alcalá, F.J.; Custodio, E. Using the Cl/Br ratio as a tracer to identify the origin of salinity in aquifers in Spain and Portugal. *J. Hydrol.* **2008**, *359*, 189–207. [CrossRef]
55. Henchiri, S.; Clergue, C.; Dellinger, M.; Gaillardet, J.; Louvat, P.; Bouchez, J. The influence of hydrothermal activity on the Li isotopic signature of rivers draining volcanic areas. *Procedia Earth Planet. Sci.* **2014**, *10*, 223–230. [CrossRef]
56. Pistiner, J.S.; Henderson, G.M. Lithium-isotope fractionation during continental weathering processes. *Earth Planet. Sci. Lett.* **2003**, *214*, 327–339. [CrossRef]
57. Vigier, N.; Decarreau, A.; Millot, R.; Carignan, J.; Petit, S.; France-Lanord, C. Quantifying Li isotope fractionation during smectite formation and implications for the Li cycle. *Geochim. Cosmochim. Acta* **2008**, *72*, 780–792. [CrossRef]
58. Wanner, C.; Sonnenthal, E.L.; Liu, X.M. Seawater δ^7Li: A direct proxy for global CO_2 consumption by continental silicate weathering? *Chem. Geol.* **2014**, *381*, 154–167. [CrossRef]
59. Marazuela, M.A.; Vázquez-Suñéa, E.; Custodio, E.; Palma, T.; García-Gile, T.; Ayora, C. 3D mapping, hydrodynamics and modelling of the freshwater-brine mixing zone in salt flats similar to the Salar de Atacama (Chile). *J. Hydrol.* **2018**, *561*, 223–235. [CrossRef]
60. Díaz, D.; Brasse, H.; Ticona, F. Conductivity distribution beneath Lascar volcano (Northern Chile) and the Puna, inferred from magnetotelluric data. *J. Volc. Geothermal Res.* **2012**, *217–218*, 21–29. [CrossRef]
61. Afanasyev, A.; Blundy, J.; Melnik, O.; Sparks, S. Formation of magmatic brine lenses via focussed fluid-flow beneath volcanoes. *Earth Planet. Sci. Lett.* **2018**, *486*, 119–128. [CrossRef]
62. Foustoukos, D.I.; Seyfield, W.E. Trace element partitioning between vapor, brine and halite under extreme phase separation conditions. *Geochim. Cosmochim. Acta* **2007**, *71*, 2056–2071. [CrossRef]
63. Tóth, J. *Gravitational Systems of Groundwater Flow—Theory, Evaluation, Utilization*; Cambridge University Press: New York, NY, USA, 2009; p. 297.

64. Hofstra, A.H.; Todorov, T.I.; Mercer, C.N.; Adams, D.T.; Marsh, E.E. Silicate melt inclusion evidence for extreme pre-eruptive enrichment and posteruptive depletion of lithium in silicic volcanic rocks of the western United States: Implications for the origin of lithium-rich brines. *Econ. Geol.* **2013**, *105*, 1691–1701. [CrossRef]
65. Benson, T.R.; Cole, M.A.; Rytuba, J.J.; Mahood, G.A. Lithium enrichment in intracontinental rhyolite magmas leads to Li deposits in caldera basins. *Nat. Commun.* **1997**, *8*, 1–9. [CrossRef]
66. Schmitt, A. Gas-saturated crystallization and degassing in large-volume, crystal-rich dacitic magmas from the Altiplano-Puna, northern Chile. *J. Geophys. Res.* **2001**, *106*, 30561–30578. [CrossRef]
67. Castor, S.B.; Henry, C.D. Lithium-Rich Claystone in the McDermitt Caldera, Nevada, USA: Geologic, Mineralogical, and Geochemical Characteristics and Possible Origin. *Minerals* **2020**, *10*, 68. [CrossRef]